AIAA JOURNAL
Vol. 42, No. 12, December 2004

Effect of Geometric Parameters on Simplex Atomizer Performance

J. Xue,* M. A. Jog,† and S. M. Jeng‡
University of Cincinnati, Cincinnati, Ohio 45221-0072
and
E. Steinthorsson§ and M. A. Benjamin¶
Parker Hannifin Corporation, Mentor, Ohio 44060

A computational analysis of flow in simplex fuel atomizers using the arbitrary-Lagrangian–Eulerian method is presented. It is well established that the geometry of an atomizer plays an important role in governing its performance. We have investigated the effect on atomizer performance of four geometric parameters, namely, inlet slot angle, spin chamber convergence angle, trumpet angle, and trumpet length. For a constant mass flow rate through the atomizer, the atomizer performance is monitored in terms of dimensionless film thickness, spray cone half-angle, and discharge coefficient. Results indicate that increase in inlet slot angle results in lower film thickness and discharge coefficient and higher spray cone angle. The spin chamber converge angle has an opposite effect on performance parameters, with film thickness and discharge coefficient increasing and the spray cone angle decreasing with increasing convergence angle. For a fixed trumpet length, the trumpet angle has very little influence on discharge coefficient. However, the film thickness decreases, and spray cone angle increases with increasing trumpet angle. For a fixed trumpet angle, the discharge coefficient is insensitive to trumpet length. Both the spray cone angle and the film thickness are found to decrease with trumpet length. Analytical solutions are developed to determine the atomizer performance considering inviscid flow through the atomizer. The qualitative trends in the variation of film thickness at the atomizer exit, spray cone angle, and discharge coefficient predicted by inviscid flow analysis are seen to agree well with computational results.

Nomenclature

A_a	=	air core area at orifice exit
A_o	=	orifice area
A_p	=	total swirl slot area
A_t	=	the trumpet end area
A_{ta}	=	air core area at the trumpet end
C_d	=	discharge coefficient, $\dot{m}/A_o(2\Delta p/\rho)^{0.5}$
D_s	=	spin chamber diameter
d_o	=	orifice diameter
d_t	=	trumpet diameter at atomizer exit
$\boldsymbol{f}$	=	body force
K	=	atomizer constant, $A_p/(D_s d_o)$
K_t	=	$A_p/(\pi r_t r_s)$
K_1	=	$A_p/(\pi r_o r_s)$
L_s	=	spin chamber length
l_o	=	orifice length
l_t	=	trumpet length
p	=	static pressure
Q	=	volume flow rate
r_i	=	radial distance from axis to inlet slot
r_o	=	orifice radius, $d_o/2$
r_s	=	spin chamber radius, $D_s/2$
r_t	=	$d_t/2$
$S(t)$	=	surface enclosing control volume $V(t)$
t	=	film thickness at exit
t^*	=	dimensionless film thickness, $t/(d_o/2)$
U	=	average total velocity at the end of orifice
$\boldsymbol{U}$	=	arbitrary velocity vector for the control volume $V(t)$
u	=	axial-velocity component
$\boldsymbol{u}$	=	velocity vector
$\bar{u}_o$	=	average axial velocity at the end of orifice
u_{oa}	=	axial velocity at the liquid–air interface at the end of orifice
$\bar{u}_t$	=	average axial velocity at the end of trumpet
u_{ta}	=	axial velocity at the liquid–air interface at the end of trumpet
$V(t)$	=	control volume
w	=	tangential velocity component
w_i	=	average tangential velocity at the inlet
$\bar{w}_o$	=	average tangential velocity at the end of orifice
w_{oa}	=	tangential velocity at the liquid–air interface at the end of orifice
$\bar{w}_t$	=	average tangential velocity at the end of trumpet
w_{ta}	=	tangential velocity at the liquid–air interface at the end of trumpet
X	=	A_a/A_o
X_t	=	A_{ta}/A_t
β	=	inlet slot angle
Δp	=	pressure drop across the nozzle
θ	=	spray cone half-angle
θ_c	=	spin chamber convergence angle
θ_t	=	trumpet angle
θ'	=	difference between spray cone half-angle and trumpet angle, $\theta - \theta_t$
ρ	=	density
τ	=	viscous stress

Presented as Paper 2002-3710 at the AIAA/ASME/SAE/ASEE 38th Joint Propulsion Conference, Indianapolis, IN, 7–10 June 2002; received 9 June 2003; revision received 16 June 2004; accepted for publication 29 June 2004.

*Ph.D. Student, Department of Mechanical, Industrial, and Nuclear Engineering.
†Associate Professor, Department of Mechanical, Industrial, and Nuclear Engineering; Milind.Jog@Uc.edu.
‡Professor, Department of Aerospace Engineering and Engineering Mechanics. Member AIAA.
§Principal Engineer, Gas Turbine Fuel Systems Division. Member AIAA.
¶Technology Team Leader, Gas Turbine Fuel Systems Division. Member AIAA.

Subscripts

i	=	parameter at the inlet
o	=	parameter at the end of orifice
oa	=	parameter at the liquid–air interface at the end of orifice
t	=	parameter at the end of trumpet
ta	=	parameter at the liquid–air interface at the end of trumpet

Introduction

PRESSURE-SWIRL atomizers (simplex atomizers) are widely used for liquid fuel atomization in gas turbine engines for propulsion and power generation applications.[1] Figure 1 shows a schematic of simplex atomizer geometry. In a simplex atomizer, the fuel is forced under high pressure to enter a swirl chamber through inlet slots at the outer wall. An air core is formed along the centerline as a result of high swirl velocity of the fuel. The fuel exits the atomizer through a small orifice with even higher swirl velocity that forces the liquid to disperse radially outward to form a hollow cone. The thin liquid sheet then becomes unstable and breaks up to form a spray of droplets.

The flow inside a simplex atomizer is turbulent, unsteady, and contains regions of recirculating flow. Additionally, the shape and the location of the liquid–air interface is unknown and must be determined as part of the solution. This poses significant difficulties in computational modeling of the flow in a simplex atomizer. Because of these difficulties, early studies of simplex atomizers employed analytical and/or experimental methods. Giffen and Muraszew[2] carried out an inviscid analysis of the flow in a simplex atomizer. They showed that the atomizer constant, which is the ratio of inlet area to the product of swirl chamber diameter and exit orifice diameter, is the most important geometric parameter of the atomizer. They derived expressions for liquid film thickness, spray cone angle, and the discharge coefficient in terms of the atomizer constant. In a practical atomizer, the flow is viscous, and other geometric parameters also influence the atomizer performance. Further developments on the effect of other geometric parameters were primarily based on experimental measurements. As described in a review by Lefebvre,[1] several semi-empirical correlations were developed that took into account the effect of length and diameter of the spin chamber and that of exit orifice. However, there is no unanimity in the predictions of film thickness and spray cone angle made by the available correlations.[3,4] Furthermore, not all geometric parameters of the atomizer have been considered in the available correlations.

As stated earlier, the high swirl velocity in pressure swirl atomizers results in an air core at the centerline of the atomizer and

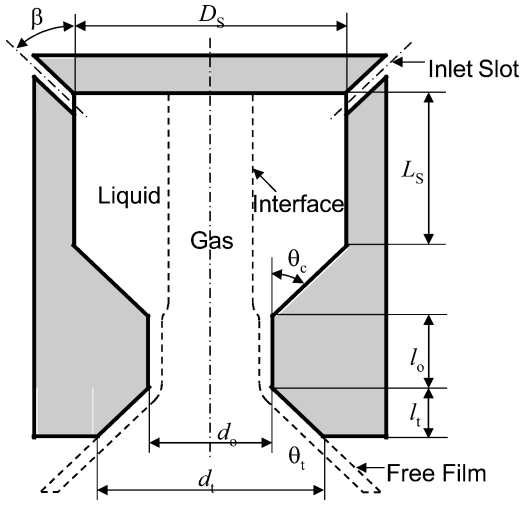

Fig. 1 Schematic of a simplex atomizer.

the position and geometry of the gas–liquid interface is not known a priori. The challenge in modeling such interaction of two fluid phases is to track their interface accurately. Modeling of motion of a liquid–gas interface is relevant to many engineering applications, and a number of methods have been used for this purpose. One approach is to treat the entire computational domain as single phase and then guess the interface by joining grid points where pressure is found to be atmospheric.[5] Solution is recalculated by creating a new grid using the calculated interface and treating the interface as a "with-slip" boundary. However, the condition of normal stress balance is not applied at the interface. Such an approach has been employed using commercially available Fluent code by Yule and Chinn.[5] The volume-of-fluid (VOF) method is another widely used method in flow simulations with multiple phases.[6] In this method the interface is represented by the fraction of cell volume occupied by the liquid. As the grid points do not exactly lie on the interface, the interface has to be reconstructed using volume fractions for each cell. In general, the accuracy strongly depends on the grid resolution around the interface, and the method can be computationally very expensive. Hansen and Madsen[7] have used this approach to simulate the flow in a simplex atomizer with commercially available CFX-4.3 code, and Dash et al.[8] have developed a code incorporating the VOF method.

To achieve accurate tracking of the interface without numerical smearing, a promising approach is to use a fully Lagrangian scheme. In this scheme each node point moves with its velocity so that the same cell mass is followed in time. Therefore, in a Lagrangian approach node points on a two-phase interface always remain on the interface, and the motion and shape of the interface can be evaluated very accurately. Such a method works well for well-behaved flows. For domains that include shear, fluid separation, and recirculation, such as the problem at hand, a Lagrangian scheme would lead to a highly distorted grid very quickly. When differential operators are calculated on a highly distorted mesh, the approximations generally lose accuracy. Furthermore, obtaining converged solutions for a complex flow on a highly distorted grid would be virtually impossible. To achieve accurate Lagrangian tracking of the interface and yet maintain mesh quality and obtain convergent solutions, we have adopted the arbitrary-Lagrangian–Eulerian (ALE)[9] method. The ALE method comprises two computational steps that combine the Lagrangian tracking with Eulerian regridding. The first step is a Lagrangian step, in which the computational grid vertices move with the same velocity as the fluid. Therefore there is no mass exchange among computational cells. The continuity and momentum conservation equations are solved using a predictor-corrector numerical scheme. The second step is an Eulerian step, in which a new adaptive grid is generated. The mass and momentum for each new cell are calculated based on the motion of new grid vertices from their Lagrangian positions. The Lagrangian step ensures that the points on the interface remain on the interface, and thus the interface is tracked accurately. The Eulerian step ensures that the grid does not get distorted, thereby maintaining solution accuracy.

We have developed a computational code to model the flow in the atomizer and to track the liquid–air interface using the ALE method.[10] To validate the developed code, experimental measurements of flowfield in the atomizer are required. However, typical pressure-swirl atomizers used in gas turbine engines are very small (exit diameter < 1 mm), and measurements of flowfield inside the atomizer are extremely difficult. To overcome this difficulty, we conducted flowfield measurements in a large-scale transparent prototype atomizer.[10,11] The large-scale prototype was designed such that parts of the atomizer could be changed to vary atomizer geometry. The experimental data for velocity field inside the atomizer, spray cone angle, film thickness, and discharge coefficient for a number of atomizer geometries were used to validate the developed code.[10,11] Experimental studies available in literature have considered four geometric parameters, namely, atomizer constant, spin chamber length-to-diameter ratio, exit orifice length-to-diameter ratio, and the ratio of spin chamber diameter to the exit orifice diameter. The validated computational model was used to conduct parametric

studies on the influence of these dimensionless geometric parameters, under constant mass flow rate[11] and constant pressure drop[12] conditions.

With the advent of new manufacturing techniques, simplex atomizers with different geometries can be produced easily. However to design such atomizers, the effect of all geometric parameters on the performance of the atomizer must be well understood. Newer designs of simplex atomizers can include inlets that are not perpendicular to the axis, and the inlet slot angle (angle β in Fig. 1) might not be 90 deg. The geometry can include a trumpet at the end of the exit orifice to limit the spray cone angle. We note that, to achieve rapid fuel air mixing, airflow can be introduced around the fuel injector through a swirler cup. In such an arrangement, it is desired to impinge the atomized fuel on the wall of a swirler cup to undergo further atomization caused by shearing action of airflow along the swirler cup wall. Therefore, in such configurations a particular spray angle is desirable rather than the maximum possible spray angle. Hence a trumpet is introduced in the atomizer geometry to limit the cone angle of the spray. Also a particular trumpet length might be needed to inject the atomized fuel at the right location in the airflow for rapid mixing. The internal convergence angle (angle θ_c in Fig. 1) might be different from 45 deg. These geometrical parameters have not been considered in studies available in literature, and the effect of variation in these parameters on the performance of simplex atomizers has not been reported in literature. None of the available semi-empirical correlations address these geometric parameters, and as such the present correlations do not provide any guidance about these parameters to atomizer designers.

The knowledge of flow in a pressure-swirl atomizer and the effect of geometric parameters on the characteristics of the liquid sheet emanating from the atomizer are extremely important to design a fuel injector. The characteristics of the liquid sheet emanating from the atomizer depend on the geometrical parameters of the atomizer, which can be expressed in dimensionless form as atomizer constant K, ratio of length to diameter of the swirl chamber L_s/D_s, that of the orifice l_o/d_o, ratio of swirl chamber to orifice diameter D_s/d_o, inlet angle β, trumpet length, trumpet angle, and the convergence angle. As described earlier, several experimental studies[1] and numerical studies[11,12] have investigated the effect of first four parameters just listed. An atomizer designer must choose a combination of geometric parameters to achieve the desired spray angle, film thickness, and discharge coefficient. Therefore, it is important to know how each geometric parameter affects the atomizer performance. Semi-empirical correlations have been developed by varying the atomizer constant L_s/D_s, l_o/d_o, and D_s/d_o and measuring their effect on atomizer performance parameters. Also, the influence of K, L_s/D_s, l_o/d_o, and D_s/d_o on atomizer performance has been studied computationally.[10–12] However, no studies that provide any guidance on the change in atomizer performance with a change in inlet slot angle, spin chamber convergence angle, trumpet angle, and trumpet length are currently available. In this paper, we have considered these four geometric parameters. The effects on atomizer performance caused by variation in these geometric parameters are computationally predicted and are shown in terms of variations of dimensionless film thickness at the atomizer exit, spray cone half-angle, and discharge coefficient. Also, analytical solutions are developed based on inviscid approximation to determine the film thickness, spray cone angle, and discharge coefficient for the atomizer.

Computational Method and Validation

As describe earlier, we have developed a computational code using the arbitrary-Lagrangian–Eulerian method. The conservation equations governing the flow are

$$\nabla \cdot \boldsymbol{u} = 0, \qquad \rho \frac{D\boldsymbol{u}}{Dt} = -\nabla P + \nabla \cdot \tau + \rho \boldsymbol{f} \tag{1}$$

Integrating Eqs. (1) over a control volume $V(t)$ with a surface $S(t)$ that moves with an arbitrary velocity and applying Leibnitz rule and Reynolds transport theorem, the equations become

$$\iint_{A(t)} (\boldsymbol{U} - \boldsymbol{u}) \cdot \mathrm{d}\boldsymbol{S} = 0$$

$$\rho \frac{\mathrm{d}}{\mathrm{d}t} \iiint_{V(t)} \boldsymbol{u} \cdot \mathrm{d}V - \iint_{A(t)} \rho \boldsymbol{u}(\boldsymbol{U} - \boldsymbol{u}) \cdot \boldsymbol{n} \, \mathrm{d}\boldsymbol{S} + \iiint_{V(t)} \nabla P \, \mathrm{d}V - \iint_{A(t)} \tau \cdot \mathrm{d}\boldsymbol{S} = 0 \tag{2}$$

Equations (2) provide the form in which the equations are used to develop the computational code. The finite volume method is used to discretize the governing integral equations, and the Baldwin–Lomax turbulence model is used to evaluate the effective viscosity.[13]

To ensure grid independence of results, the code was run for several flow conditions with different grid densities. Two sets of results for the same flow conditions and geometry are shown in Table 1 with 80×21 and 159×41 grid points, respectively. The difference in results between the two grids is small and indicates that an 80×21 or similar grid is sufficient to get accurate results.[12]

Table 1 Results for two different grid densities

Parameter	Grid 1 (80×21)	Grid 2 (159×41)
t, mm	0.5378	0.5322
u_{av}, m/s	24.20	24.51
w_{av}, m/s	19.15	19.32
C_d	0.4350	0.4505
θ, deg	38.35	38.25

Table 2 Comparison of computational results with experimental measurements

Case	Parameter	Experimental	CFD
1	t, mm	2.68	2.633
	θ, deg	42.90	41.26
	C_d	0.2781	0.2678
2	t, mm	2.68	2.544
	θ, deg	39.35	42.26
	C_d	0.2821	0.2517
3	t, mm	2.64	2.542
	θ, deg	40.35	42.40
	C_d	0.2721	0.2504

The developed computational-fluid-dynamics (CFD) model based on the ALE method was validated by comparison with experimental data for a velocity variation inside the atomizer as well as measurements for spray cone angle, film thickness, and discharge coefficient using a large-scale atomizer. Typical pressure-swirl atomizers used in gas turbine engines are very small (exit diameter < 1 mm), and measurements of flowfield inside the atomizer are extremely difficult. To overcome this difficulty, we conducted flowfield measurements in a large-scale transparent prototype atomizer.[10,11] The large-scale prototype was designed such that parts of the atomizer could be changed to vary atomizer geometry.[10,11,14] The particle-image-velocimetry technique, charge-coupled-device camera, and ultrasonic sensors were used for measurements of velocity field, spray cone angle, and film thickness at the atomizer exit, respectively, in large-scale prototype atomizers. The uncertainty in the measurements is about 5% for discharge coefficient, about 2 deg in spray angle, and less than 10% in film thickness measurements. Table 2 shows a comparison of computational predictions of film thickness, spray angle, and discharge coefficient with experimental measurements for three cases. It is seen that the computational results agree very well with the experimental measurements within experimental accuracy. The geometric and flow parameters for the three cases were $L_s = 89$ mm, $D_s = 76$ mm, $d_o = 21$ mm, $l_o = 5$ mm, $A_p = 406$ mm^2, and $\beta = 90$ deg. Flow rate in case 1 was 0.95 kg/s, 0.95 kg/s for case 2, and 1.25 kg/s for case 3.

Results and Discussion

We have investigated the effect of four geometric parameters, namely, inlet slot angle β, spin chamber convergence angle θ_c, trumpet angle θ_t, and ratio of trumpet length to orifice diameter l_t/d_o, on the performance of pressure-swirl atomizers. The variation in the atomizer performance is presented in terms of the dimensionless liquid film thickness at the exit of the orifice t^*, spray cone half-angle θ, and discharge coefficient C_d. All cases were run keeping mass flow rate constant. When one parameter was changed, all other geometric parameters were held constant.

Effect of Variation in Inlet Slot Angle β

To investigate the effect of inlet slot angle, we used an atomizer geometry without a trumpet. The dimensionless film thickness, spray cone half-angle, and discharge coefficient are plotted in Figs. 2a and 2b with variation in inlet slot angle. The film thickness was determined from the CFD results at the orifice exit. In the numerical method used here, the interface between liquid and gas is tracked as a sharp interface, and therefore the CFD results directly provide the film thickness. The discharge coefficient is calculated based on the pressure drop between in inlet and exit of the atomizer obtained in the numerical solution. With a fixed mass flow rate through the atomizer, a change in inlet slot angle results in a change in the ratio of inlet axial to swirl velocity components. With $\beta = 90$ deg the fuel has no axial-velocity component at the inlet. Hence for the same mass flow rate, $\beta = 90$ deg gives greater swirl velocity compared to $\beta = 40$ deg case.

Figure 2a shows that with an increase of β from 40 to 90 deg, dimensionless thickness t^* decreases about 25%, discharge coefficient C_d decreases about 35%, and spray cone half-angle θ increases by about 15%. The higher swirl velocity that corresponds to a higher inlet slot angle pushes the liquid to the atomizer walls, and the liquid film thickness in the exit orifice decreases. The spray cone angle is governed by the ratio of axial-to swirl-velocity components at the exit. The cone angle is seen to increase with inlet slot angle. This is because of the larger centrifugal force caused by the higher swirl-velocity component. As the mass flow rate is kept constant, thinner liquid film in the exit orifice section corresponds to higher axial velocity. A combination of increased swirl and axial velocity leads to a higher pressure drop across the atomizer, and the discharge coefficient decreases. As evident from Fig. 2a, the changes in spray cone angle, discharge coefficient, and film thickness are large,

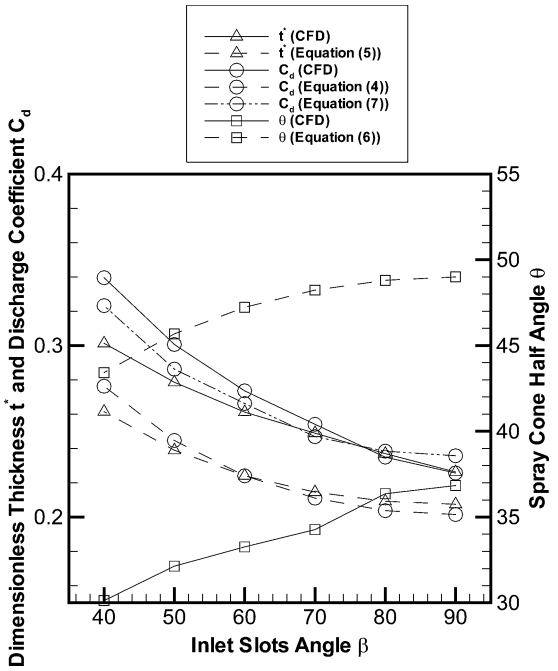

Fig. 2a Variation of atomizer performance parameters with inlet slots angle β.

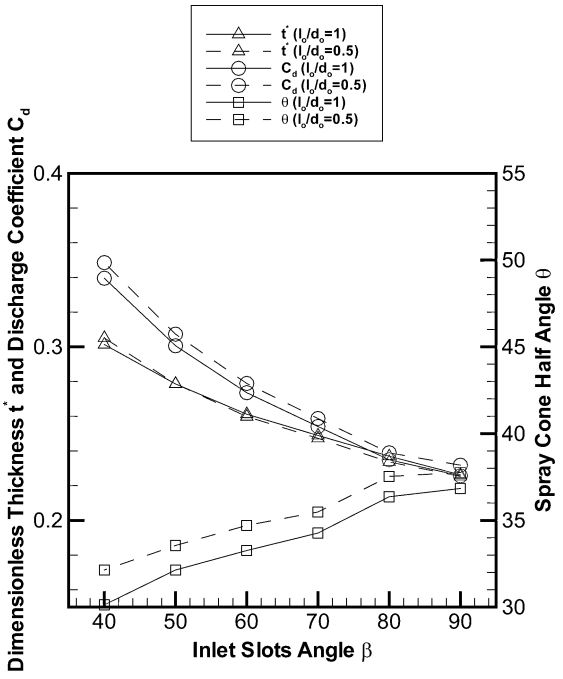

Fig. 2b Comparison of results for $l_o/d_o =$ ——, 1 and - - - -, 0.5.

indicating that inlet angle is an important parameter that significantly influences the performance of the atomizer. Empirical correlations available in the literature do not include the inlet slot angle and are unable to predict its influence on atomizer performance.

Analysis can be carried out using inviscid theory to examine the effect of the inlet slot angle. We have modified the inviscid analysis of Giffen and Muraszew[2] to include the inlet slot angle. The details are given in the Appendix. Only the final equations are given here:

$$K^2 = (\pi^2/32)[(1 - X)^3/X^2](r_i/r_s)^2 \sin^2 \beta \tag{3}$$

$$C_d = [(1 - X)^3/(1 + X)]^{0.5} \tag{4}$$

From the definition of X, we get

$$t^* = 1 - \sqrt{X} \tag{5}$$

$$\sin\theta = \frac{(\pi/2)C_d \sin\beta}{K\left(1 + \sqrt{X}\right)}\left(\frac{r_i}{r_s}\right) \tag{6}$$

Equation (4) is similar to one obtained by Giffen and Muraszew; however, the effect of inlet slot angle is apparent in Eq. (3). The results of Eqs. (3), (4), and (6) are plotted in Fig. 2a using dashed lines. For film thickness, comparing with the CFD results, it is seen that the analytical inviscid solution provides the correct qualitative variation but predicts lower values. This is to be expected as the inviscid theory does not account for the viscous effects that would tend to decrease the velocity and increase film thickness.

Equation (4) predicts lower values for the discharge coefficient than the computational results. Giffen and Muraszew[2] also observed this trend in comparison with available experimental data. They modified their equation by introducing a coefficient A as shown next and suggested $A = 1.17$ based on experimented data:

$$C_d = A[(1 - X)^3/(1 + X)]^{0.5} \tag{7}$$

It is seen in Fig. 2a that our computational results match well with this modified equation [Eq. (7)].

There is a significant difference in the prediction of spray cone angle using inviscid approximation and numerical results. The numerical results are based on the solution of Navier–Stokes equations, which fully account for viscous forces. Because of the accounting of viscous forces, difference in the predictions of CFD results and

those with inviscid approximation (theoretical results) is to be expected. Furthermore, the spray angle is governed by the ratio of the average swirl to the average axial velocity at the atomizer exit. More precisely, it is related to the tan inverse of the average swirl-to axial-velocity ratio. A change in this ratio will change the spray angle. For the cases considered here, the decrease in swirl velocity compared to inviscid prediction is larger compared to the decrease in the axial velocity. Hence the inviscid results overpredict the spray angle. Our earlier experiments[10] also show considerable difference between experimental measurements and inviscid analysis for spray angle, with inviscid theory overpredicting the spray angle compared to experimental measurements, consistent with the CFD results.

The equations derived using inviscid approximation [Eqs. (3–6)] do not account for variation in all geometric parameters. For example, the ratio of length to diameter of the swirl chamber L_s/D_s, that of the orifice l_o/d_o influence the spray angle; however, these parameters do not appear in Eqs. (3–6) at all. Numerical results obtained with a different values of L_s/D_s (or l_o/d_o) will be different, but the inviscid predictions will remain the same. Therefore, for different values of L_s/D_s (or l_o/d_o) the difference between numerical results and inviscid approximation will be different. This is seen in Fig. 2b, where results for spray cone angle, discharge coefficient, and film thickness at exit are presented for $l_o/d_o = 0.5$ and $l_o/d_o = 1$. We note that the variations in atomizer performance parameters with β, for the two values of l_o/d_o, are essentially parallel. This makes the results very useful in designing simplex atomizers.

Effect of Variation in Trumpet Angle θ_t

Note in this study the length of the trumpet l_t has been held constant as θ_t is varied. Figure 3 indicates that as θ_t increases from 10 to 40 deg, dimensionless thickness t^* decreases about 42%, spray cone half-angle θ increases from 22 to 40 deg, but discharge coefficient C_d remains almost constant. This shows that the trumpet can be very effective in controlling the spray cone angle and the film thickness without significantly affecting the pressure drop across the atomizer. As pressure drop across the atomizer remains relatively steady, the axial velocity at the end of the exit orifice is expected to exhibit little variation. However, trumpet diameter d_t increases with increase in θ_t so that the film thickness t^* decreases when the flow rate through the atomizer is kept constant.

Considering inviscid flow through the atomizer, we have developed analytical solutions for film thickness, spray cone half-angle, and the discharge coefficient for an atomizer geometry with trumpet. Detailed analysis and a schematic of the geometry are provided in the Appendix. The final equations are

$$(A_o/A_t)^2\left[1\Big/\cos^2\theta_t(1-X_t)^2 + \left(1\Big/K_t^2X_t\right)(r_i/r_s)^2\sin^2\beta\right] = 1\Big/C_d^2 \tag{8}$$

where

$$X_t = A_{\text{ta}}/A_t, \qquad K_t = A_p/\pi r_t r_s$$

$$t^* = \left(1-\sqrt{X_t}\right)(r_t/r_o)\cos\theta_t \tag{9}$$

$$\theta = \theta_t + \theta' \tag{10}$$

where

$$\tan\theta' = \left[2\left(1-\sqrt{X_t}\right)\Big/K_t\right](r_i/r_s)\sin\beta\cos\theta_t$$

Results using Eqs. (8–10) are shown in Fig. 3 with dashed lines. Once again the trends shown by the analytical solutions are seen to match well with computational results. Similar to Fig. 2, the analytical inviscid solutions give lower values of film thickness and discharge coefficient and higher values of spray cone half-angle. The results of Eq. (4) underpredict the discharge coefficient. The modified Eq. (7) provides improved match with the numerical results. As stated earlier, the differences in inviscid solutions and numerical results can be attributed to omission of viscous forces in the inviscid treatment. Compared to inviscid flow through the atomizer, the decrease in average axial velocity as a result of viscous forces is less than the reduction in average swirl velocity resulting in lower values of spray cone half-angle.

Effect of Variation of Dimensionless Trumpet Length l_t/d_o

To study the effect of variation trumpet length, both orifice diameter d_o and trumpet angle θ_t are held constant as l_t is varied. Figure 4 indicates that with an increase in l_t/d_o dimensionless thickness t^* decreases about 14%, discharge coefficient shows virtually no

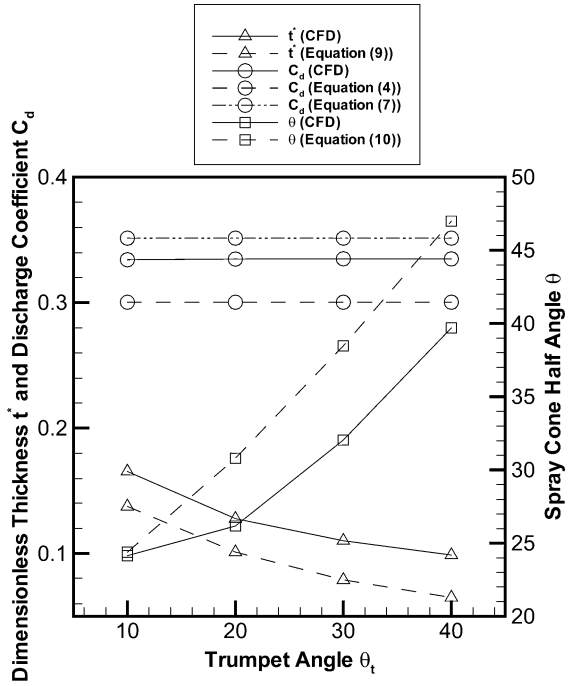

Fig. 3 Variation of atomizer performance parameters with trumpet angle θ_t.

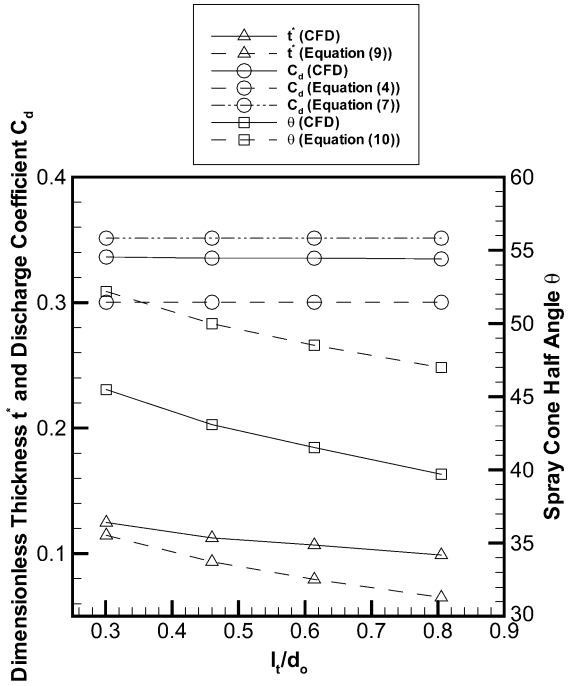

Fig. 4 Variation of atomizer performance parameters with ratio of trumpet length to orifice diameter l_t/d_o.

change, whereas spray cone half-angle decreases about 9% for the range of dimensionless trumpet length considered here. For constant flow rate across the atomizer, the pressure drop across the atomizer and the axial velocity at the end of the exit orifice are not expected to change significantly with a change in the trumpet length. As such, the discharge coefficient shows very little change with trumpet length. However, as the trumpet length increases, to keep the flow cross-sectional area relatively constant the film thickness decreases. Also, as the trumpet diameter increases, the principle of conservation of angular momentum dictates that the liquid swirl velocity would decrease as it moves along the trumpet length. Therefore, the spray cone angle is seen to decrease with increasing trumpet length. Equations (8–10) just outlined provide atomizer performance parameters for inviscid flow through the atomizer. Although the trumpet length does not directly appear in Eqs. (8–10), we note that for a fixed trumpet angle X_t is a function of the trumpet length. The effects of variation in trumpet length for inviscid flow are plotted in Fig. 4 with dashed lines. Similar to inviscid flow solutions for variations in inlet slot angle and trumpet angle, the values for film thickness and discharge coefficient predicted with computational model are higher than analytical solutions, and those of spray angle are lower than analytical solutions. The results for discharge coefficient using a modified Eq. (7) are significantly closer to computational results.

Effect of Variation in Spin Chamber Convergence Angle θ_c

In this case, the geometry of the atomizer is one without trumpet, and all geometric parameters have been kept fixed except for θ_c. As seen from Fig. 5, for the atomizer configuration considered in this study, with an increase in θ_c from 45 to 90 deg, dimensionless thickness t^* increases about 16%, C_d increases about 34%, and spray cone half-angle θ decreases about 9%. Earlier studies have shown[10,12] that the flowfield inside a simplex atomizer has a region of recirculating flow. The majority of the liquid entering from the inlet slots flows through a region close to the liquid–gas interface and enters the orifice. The location and size of the recirculating flow affects the axial-velocity variations in the spin chamber and consequently in the exit orifice. As the convergence angle changes, the recirculating region in the spin chamber can change considerably. This is illustrated in Figs. 6a and 6b, which show flow streamlines for two atomizer geometries with convergence angle 60 and 90 deg, respectively. As the flow structure changes, the velocity variation in the atomizer is altered, and consequently the film thickness at the exit, spray cone half-angle, and discharge coefficient change.

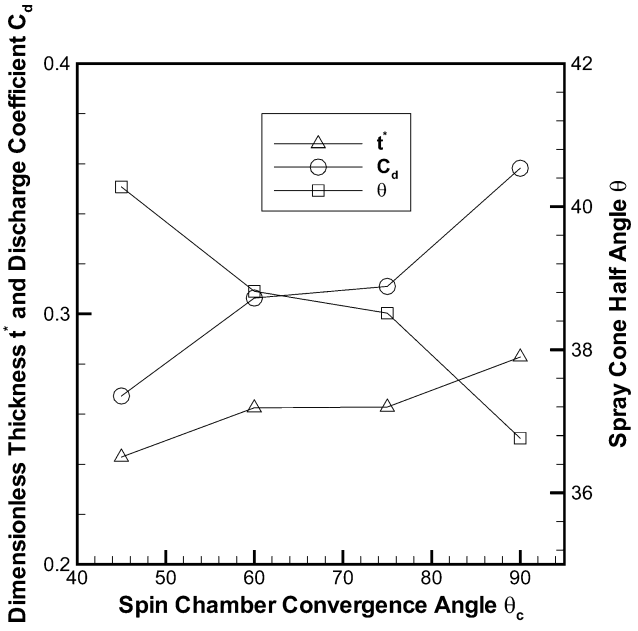

Fig. 5 Variation of atomizer performance parameters with convergence angle θ_c.

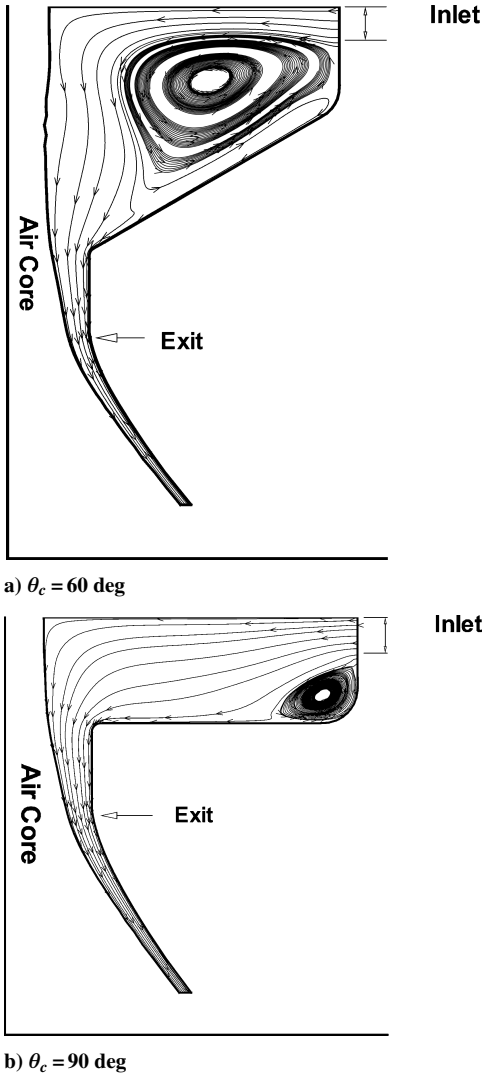

Fig. 6 Streamlines for flow inside the atomizer for different θ_c. Inlet slot angle $\beta = 90$ deg.

Although the spray angle is lowest and the film thickness is largest at convergence angle of 90 deg, this geometry might be preferred in some cases as it is easier and less expensive to manufacture compared to the geometry with smaller convergence angle. The effects caused by changes in spin chamber convergence angle cannot be predicted by inviscid analysis.

Conclusions

We have used a computational model based on the arbitrary-Lagrangian–Eulerian method to predict the flow in a simplex atomizer. The effect of four geometric parameters on the atomizer performance was investigated. The four geometric parameters considered were the inlet slot angle, trumpet angle and length, and the spin chamber convergence angle. The atomizer performance is shown in terms of variations of dimensionless film thickness, spray cone half-angle, and discharge coefficient. Results indicate that increase in inlet slot angle results in lower film thickness and discharge coefficient and higher spray cone angle. The spin chamber convergence angle has an opposite effect on performance parameters. With an increase in convergence angle, film thickness and discharge coefficient increase, whereas the spray cone angle decreases. The trumpet angle has very little influence on discharge coefficient. However, the film thickness decreases, and spray cone angle increases with increasing trumpet angle. The discharge coefficient is insensitive to trumpet length, whereas both the spray cone angle and the film thickness decrease with increasing trumpet length. The effect of the geometric parameters has not been reported in the literature, and as such

the results presented here will provide useful guidance in designing simplex atomizers.

Appendix: Inviscid Analysis for Pressure Swirl Atomizers

The analysis closely follows the development by Giffen and Muraszew[2] with appropriate additions for the new geometric parameters considered here. First we consider the effect of inlet slot angle for an atomizer without trumpet. Here we consider a more general case where the inlet is not necessarily at $r = r_s$, as shown in Fig. A1.

In pressure swirl atomizer, the liquid flow can be considered as a spiral motion as a result of an axial flow being superimposed on a free vortex.

For a free vortex,

$$wr = w_i r_i = \text{constant} \tag{A1}$$

where

$$w_i = Q \sin\beta / A_p \tag{A2}$$

According to Bernoulli's equation, the total pressure (injection pressure) in the liquid flowing through the orifice is

$$\Delta P = p + \tfrac{1}{2}\rho u^2 + \tfrac{1}{2}\rho w^2 = \text{constant} \tag{A3}$$

where p is the static pressure. At the air core, $p = 0$. So,

$$\Delta P = \tfrac{1}{2}\rho u_{\text{oa}}^2 + \tfrac{1}{2}\rho w_{\text{oa}}^2 \tag{A4}$$

and the axial velocity can be calculated as

$$u_{\text{oa}} = Q/(A_o - A_{\text{oa}}) \tag{A5}$$

According to Eqs. (A1) and (A2),

$$w_{\text{oa}} = \frac{Q r_i \sin\beta}{A_p r_{\text{oa}}} \tag{A6}$$

Substituting into Eq. (A3) u and w from Eqs. (A5) and (A6),

$$\Delta P = \frac{1}{2}\rho\left[\left(\frac{Q}{A_o - A_{\text{oa}}}\right)^2 + \left(\frac{Q r_i \sin\beta}{A_p r_{\text{oa}}}\right)^2\right] \tag{A7}$$

From the definition of C_d, we get

$$Q = C_d A_o (2\Delta P/\rho)^{0.5} \tag{A8}$$

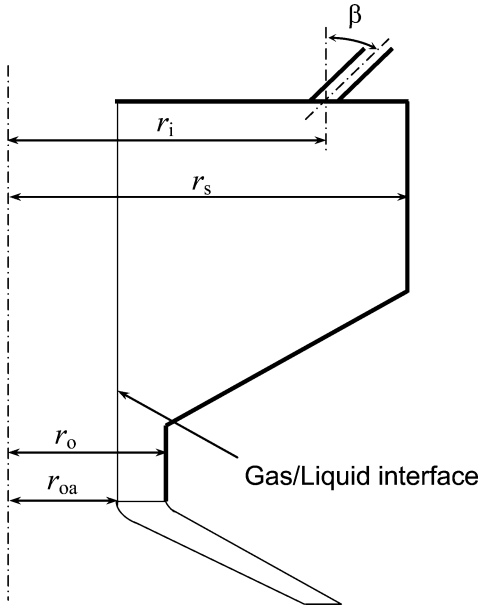

Fig. A1 Schematic of pressure swirl atomizer.

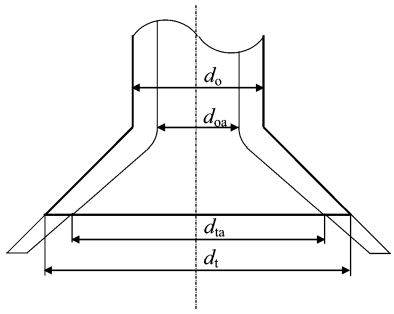

Fig. A2 Schematic of orifice with trumpet.

Substitution of Q from Eq. (A8) into Eq. (A7),

$$1/C_d^2 = 1/(1-X)^2 + \left(1/K_1^2 X\right)(r_i/r_s)^2 \sin^2\beta \tag{A9}$$

where

$$X = A_{\text{oa}}/A_o, \qquad K_1 = A_p/\pi r_o r_s$$

Assume that the size of the air core in the orifice will be such as to give maximum flow. That means C_d is maximum:

$$\frac{\mathrm{d}\left(1/C_d^2\right)}{\mathrm{d}X} = 0 \Rightarrow K_1^2 = \frac{(1-X)^3}{2X^2}\left(\frac{r_i}{r_s}\right)^2 \sin^2\beta \tag{A10}$$

Substitute Eq. (A10) into Eq. (A9):

$$C_d = [(1-X)^3/(1+X)]^{0.5} \tag{A11}$$

$$\because K = A_p/d_s d_o \Rightarrow K = (\pi/4)K_1 \tag{A12}$$

Substitute Eq. (A12) into Eq. (A10):

$$K^2 = (\pi^2/32)[(1-X)^3/X^2](r_i/r_s)^2 \sin^2\beta \tag{A13}$$

From the definition of X, we get

$$t^* = 1 - \sqrt{X} \tag{A14}$$

Following Giffen and Muraszew,[2] for the spray cone half-angle θ we have

$$\tan\theta = \bar{w}_o/\bar{u}_o \qquad \text{or} \qquad \sin\theta = \bar{w}_o/U \tag{A15}$$

$$\because Q = C_d A_o U \Rightarrow U = Q/C_d A_o \tag{A16}$$

At the exit, the total angular momentum in the orifice

$$\int_{r_{\text{oa}}}^{r_o} (2\pi r \rho \bar{u}_o dr)\frac{Q r_i}{A_p r}\sin\beta = \frac{2\pi\rho\bar{u}_o Q r_i (r_o - r_{\text{oa}})}{A_p}\sin\beta \tag{A17}$$

The total mass flow in the orifice

$$\rho\bar{u}_o(A_o - A_{\text{oa}}) \tag{A18}$$

$\Rightarrow$ mean tangential velocity at the exit

$$\bar{w}_o = \frac{2\pi\, Q r_i (r_o - r_{\text{oa}})\sin\beta}{A_p(A_o - A_{\text{oa}})} \tag{A19}$$

Substituting Eqs. (A16) and (A19) into Eq. (A15), we get

$$\sin\theta = \frac{(\pi/2)C_d \sin\beta}{K\left(1+\sqrt{X}\right)}\left(\frac{r_i}{r_s}\right) \tag{A20}$$

Now we consider an atomizer geometry with trumpet, as shown in Fig. A2.

Following the foregoing analysis, consider the air core at the trumpet end, and we have

$$u_{\text{ta}} = \frac{Q}{(A_t - A_{\text{ta}})\cos\theta_t} \tag{A21}$$

$$w_{\text{ta}} = \frac{Qr_i \sin\beta}{A_p r_{\text{ta}}} \tag{A22}$$

$$\Rightarrow \Delta P = \frac{1}{2}\rho\left[\left(\frac{Q}{(A_t - A_{\text{ta}})\cos\theta_t}\right)^2 + \left(\frac{Qr_i \sin\beta}{A_p r_{\text{ta}}}\right)^2\right] \tag{A23}$$

Substitution of Q from Eq. (A8) into Eq. (A23),

$$(A_o/A_t)^2\left[1\Big/\cos^2\theta_t(1 - X_t)^2 + \left(1\Big/K_t^2 X_t\right)(r_i/r_s)^2 \sin^2\beta\right] = 1\Big/C_d^2 \tag{A24}$$

where

$$X_t = A_{\text{ta}}/A_t, \qquad K_t = A_p/\pi r_t r_s$$

$$\Rightarrow t^* = \left(1 - \sqrt{X_t}\right)(r_t/r_o)\cos\theta_t \tag{A25}$$

For the spray cone half-angle θ, approximately we have

$$\theta = \theta_t + \theta' \tag{A26}$$

where

$$\tan\theta' = \frac{\bar{w}_t}{\bar{u}_t} \tag{A27}$$

the mean velocity along with the trumpet direction at the trumpet end

$$\bar{u}_t = Q/(A_t - A_{\text{ta}})\cos\theta_t \tag{A28}$$

At the trumpet end, the total angular momentum

$$\int_{r_{\text{ta}}}^{r_t} (2\pi r\rho\bar{u}_t \cos\theta_t \, \mathrm{d}r)\frac{Qr_i}{A_p r}\sin\beta = \frac{2\pi\rho\bar{u}_t \cos\theta_t Qr_i(r_t - r_{\text{ta}})}{A_p}\sin\beta \tag{A29}$$

The total mass flow at the trumpet end

$$\rho\bar{u}_t \cos\theta_t(A_t - A_{\text{ta}}) \tag{A30}$$

$\Rightarrow$ mean tangential velocity at the trumpet end

$$\bar{w}_t = \frac{2\pi Qr_i(r_t - r_{\text{ta}})\sin\beta}{A_p(A_t - A_{\text{ta}})} \tag{A31}$$

Substituting Eqs. (A28) and (A31) into Eq. (A27), we get

$$\tan\theta' = \left[2\left(1 - \sqrt{X_t}\right)\Big/K_t\right](r_i/r_s)\sin\beta\cos\theta_t \tag{A32}$$

Acknowledgments

The support of this work by Parker Hannifin Corp., the National Science Foundation, and the University Research Council of the University of Cincinnati is thankfully acknowledged.

References

[1]Lefebvre, A. H., *Atomization and Spray*, Hemisphere, New York, 1989.

[2]Giffen, E., and Muraszew, A., *The Atomization of Liquid Fuels*, Wiley, New York, 1953.

[3]Benjamin, M. A., Jeng, S. M., and Jog, M. A., "Comparison of Simplex Atomizer Correlations with Detailed CFD and Experimental Data," *Proceedings of the Tenth Annual Conference on Liquid Atomization and Spray Systems*, Inst. for Liquid Atomization and Spray Systems—Americas, Irvine, CA, 1997, pp. 45–49.

[4]Liao, Y., Sakman, A. T., Jeng, S. M., Jog, M. A., and Benjamin, M. A., "A Comprehensive Model to Predict Simplex Atomizer Performance," *Journal of Engineering for Gas Turbines and Power*, Vol. 121, No. 2, 1999, pp. 285–294.

[5]Yule, A. J., and Chinn, J. J., "Pressure Swirl Atomizer Internal Flow and Performance," *Proceedings of the Tenth Annual Conference on Liquid Atomization and Spray Systems*, Inst. for Liquid Atomization and Spray Systems—Americas, Irvine, CA, 1997, pp. 205–209.

[6]Steinthorsson, E., and Lee, D. M., "Numerical Simulations of Internal Flow in a Simplex Atomizer," *Eighth International Conference on Liquid Atomization and Spray Systems* [CD-ROM], Inst. for Liquid Atomization and Spray Systems—Americas, Irvine, CA, 2000.

[7]Hansen, K. S., and Madsen, J., "A Computational and Experimental Study of the Internal Flow in a Scaled Pressure-Swirl Atomizer," M.Sc. Thesis, Aalborg Univ., Esbjerg, Denmark, June 2001.

[8]Dash, S. K., Halder, M. R., Peric, M., and Som, S. K., "Formation of Air Core in Nozzles with Tangential Entry," *Journal of Fluids Engineering*, Vol. 123, No. 4, 2001, pp. 829–835.

[9]Hirt, C. W., Amsden, A. A., and Cook, J. L., "An Arbitrary Lagrangian-Eulerian Computing Method for All Flow Speeds," *Journal of Computational Physics*, Vol. 14, No. 3, 1974, pp. 227–253.

[10]Jeng, S. M., Jog, M. A., and Benjamin, M. A., "Computational and Experimental Study of Liquid Sheet Emanating from Simplex Fuel Nozzle," *AIAA Journal*, Vol. 36, No. 2, 1998, pp. 201–207.

[11]Sakman, A. T., Jog, M. A., Jeng, S. M., and Benjamin, S. M., "Parametric Study of Simplex Fuel Nozzle Internal Flow and Performance," *AIAA Journal*, Vol. 38, No. 7, 2000, pp. 1214–1218.

[12]Xue, J., Jog, M. A., Jeng, S. M., Steinthorsson, E., and Benjamin, M. A., "Influence of Geometry on the Performance of Simplex Nozzles Under Constant Pressure Drop," *Proceedings of the Fifteenth Annual Conference on Liquid Atomization and Spray Systems* [CD-ROM], Inst. for Liquid Atomization and Spray Systems—Americas, Irvine, CA, 2002.

[13]Baldwin, B. S., and Lomax, H., "Thin-Layer Approximation and Algebraic Model for Separated Turbulent Flows," AIAA Paper 78-257, Jan. 1978.

[14]Holtzclaw, D., Sakman, T., Jeng, S. M., Jog, M. A., and Benjamin, M. A., "Investigation of Flow in a Simplex Fuel Nozzle," AIAA Paper 97-2970, July 1997.

S. Aggarwal
Associate Editor